RSC Advances

PAPER

View Article Online
View Journal | View Issue

Cite this: *RSC Adv.*, 2023, **13**, 33062

Carbon nanotube papers with p–n junctions along the thickness direction†

Hsin-Jung Tsai, Ling-Hung Chou, Ping-Chun Chen, Yung-Kai Yang and Wen-Kuang Hsu *

Received 6th July 2023
Accepted 3rd November 2023

DOI: 10.1039/d3ra04503j

rsc.li/rsc-advances

Conductive papers made from carbon nanotubes and wood fibers exhibit a p-type character. N_2 plasma treatment converts paper into n-type and conversion is verified by elemental analyses, work function and Hall-effect measurements. By screening one face of p-type paper in plasma, the p–n junctions are successfully created along the thickness direction and electrical rectification is evident by current–voltage measurement.

1 Introduction

Diodes are two-terminal electronic devices made of different semiconductor materials (*e.g.* p–n junction).[1,2] Accordingly, a built-in-potential (ΔE) forms at the interface where bands bend and Fermi levels (E_F) equalize. This junction barrier, also known as the depletion layer (DL), becomes thinned in forward bias thus allowing current to flow. Application of reverse bias, in contrast, widens the DL so current cannot pass until breakdown.[3] Electrical rectification is also present in hetero-junction nanowires and doped nanostructures; the former is produced through catalytic pyrolysis of hydrocarbons and is verified to be Schottky type.[4] The latter is of p–n type where the DL is made by coating of polymers onto carbon nanotubes (CNTs).[5]

CNTs are one-dimensional conductors made of rounded graphite sheets and can be made in a large quantity through different means.[5] The electronic properties of CNTs are peculiar in that the band structure is determined by tube diameter (d) and chirality (θ) expressed as $d = (3)^{1/2} \times a_{c-c} (m^2 + mn + n^2)^{1/2}/\pi$ and $\theta = \tan^{-1}[3^{1/2} \times m/(2n + m)]$ where a_{c-c}, n and m are C–C bond length (=1.42 Å) and integers. For a given (n, m), metallic tubes satisfy $2n + m = 3q$ (q: integer) and $2n + m \neq 3q$ for semiconducting CNTs with the band gap approximating $E_g = \varphi \times a_{c-c}/d$ ($\varphi = 3$ eV).[6] However, creation of electronic devices on individual CNTs remains unfavourable thus far; first, current techniques cannot make CNTs with similar d and θ so band structure appears to vary from tube to tube;[7] second, CNTs either made by catalytic pyrolysis of hydrocarbons or electrical arc discharge of graphite do not have all sp^2 valencies satisfied so electronic properties are actually governed by localized states around band edges, *e.g.* functionalized and doped lattices.[8–10] In this work, we demonstrate the production of CNT papers with p–n junctions along the thickness direction where ΔE is created by N_2 plasma. Papers are flexible and can be scaled up to cm^2 dimension for practical use, *e.g.* voltage doubling and output smoothing.[3]

2 Experimental

2.1. Production of p-type CNTs conductive paper

As-made CNTs behave as p-type in air and are therefore used as starting materials (multi-walled, 8–35 μm in length, 3–40 nm in diameter, 85–95% purity, Conjutek, Taiwan).[11] However, bulk CNTs are in powder form and cannot firmly bind together without plastic binders. In order to avoid use of plastics the CNTs are mixed with wood fibres (WFs, *i.e.* plant-based tissue paper with $CaCO_3$ < 5 wt%).[12] First, CNTs are ultrasonically dispersed in deionized water (200 ml) and suspension is poured into a blender (rpm = 1500 and power = 1200 W, i → ii, Fig. 1a). Second, tissue paper is added into CNT suspension and the mixture is stirred for 10 min, followed by filtering in a vacuum-suction system and hot-pressing (50 kg cm^{-2}, 30 min) to form flexible CNTs-WF papers hereafter defined as p-CNT-WF (iii–v, Fig. 1a). Paper dimension is 150 × 150 × 0.3 mm and the filling fraction (f_{CNT}) of CNTs in WF is set at 1, 10, 20, 30 and 40 wt%.

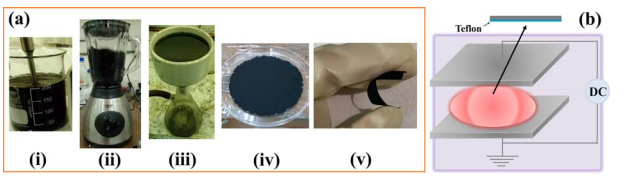

Fig. 1 Production of p-CNT-WF (a) and creation of p–n junctions across p-CNT-WF by N_2 plasma treatments (b). Teflon coverage is denoted by arrow.

Department of Materials Science and Engineering, National Tsing-Hua University, Hsinchu, 30013, Taiwan. E-mail: wkhsu@mx.nthu.edu.tw

† Electronic supplementary information (ESI) available. See DOI: https://doi.org/10.1039/d3ra04503j

2.2. Production of B-doped CNTs conductive paper

Conductive papers are also made from boron-doped multi-walled CNTs (B-CNTs) known as an enhanced p-type with hole carrier density 5–6 times greater than un-doped.[13] First, B_2O_3 powder (2 g) and CNTs (6 g) are ultrasonically mixed in deionized water (200 ml) and suspension is dried in an oven (60 °C). Second, the mixture is heated to 1200 °C in Ar flow (100 sccm) for 4 h, followed by methanol (100 ml, 1 h) rinsing to remove residual oxides (*i.e.* $2B_2O_3 + 15C \rightarrow 4BC_3 + 3CO_2$).[14] Third, B-CNT-WF is made according to same procedures described in Fig. 1a.

2.3. Creation of p–n junctions across p-CNT-WF thickness

The non-thermal equilibrium plasma operates at room temperature and is widely used for a variety of chemical purposes, *e.g.* surface cleaning and modification.[15,16] The N_2 plasma is used to create p–n junctions across the p-CNT-WF thickness according to following procedures. First, one face of a p-CNT-WF is covered with Teflon film (Fig. 1b). Second, one-face screened paper is subjected to N_2 plasma at 0.3 torr and 180 V for 10–20 min. Plasma treated papers are hereafter defined as p-CNT-WF/n-CNT-WF$_{(t)}$ where slash denotes interface between Teflon protected (*i.e.* p-CNT-WF) and plasma treated faces (n-CNT-WF) and, the subscript t denotes plasma treating time. Similar procedures are also applied to B-CNT-WF and resultant papers are defined as B-CNT-WF/n-CNT-WF$_{(t)}$.

2.4. Electrical resistivity measurements of p-CNT-WF

Electrical resistivity (ρ) of p-CNT-WF is measured by van der Pauw technique (*i.e.* four-terminal method) which excludes contact resistance and determines paper resistance (R) according to equation $e^{(-\pi aR_1/\rho)} + e^{(-\pi aR_2/\rho)} = 1$ where $R_1 = V_{DC}/I_{AB}$, $R_2 = V_{AD}/I_{BC}$ and a is paper thickness (=0.3 mm, Fig. 2a).[17] Measurements are carried out on papers made of different f_{CNT} so the electrical percolation threshold (η) and optimal f_{CNT} for making p–n junctions can be determined.

2.5. Two-terminal measurements of p-CNT-WF/n-CNT-WF$_{(t)}$ and B-CNT-WF/n-CNT-WF$_{(t)}$

The *I–V* characters of p-CNT-WF/n-CNT-WF and B-CNT-WF/n-CNT-WF are studied by two-terminal DC technique (Keithley, Source meter 2450 & Agilent B1500A). First, two electrical leads are glued to both faces of p-CNT-WF/n-CNT-WF respectively using conductive Ag paste (Fig. 2b). Second, the forward and reverse bias measurements are carried out at ±5 V to determine threshold voltage (V_{th}), maximum forward current (I_F) and ratio of reverse to forward resistance (R_R/R_F) where $R_R/R_F \approx 1$ for ohmic conductor (*i.e.* symmetric *I–V* profile) and $R_R/R_F > 1$ for polarized conductors.[3] Third, all measurements are performed in a chamber with relative humidity and temperature controlled at 25–30% and 25 °C to evade water doping.[18]

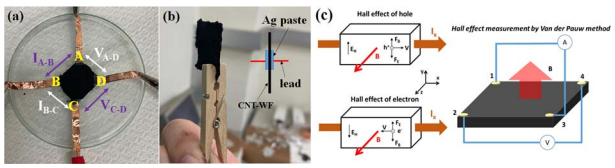

Fig. 2 Four-terminal measurements for p-CNT-WF made of different f_{CNT} (a) and two-terminal measurements for p-CNT-WF/n-CNT-WF and B-CNT-WF/n-CNT-WF (b). Schematic diagram of Hall effect (left) and the Hall effect measurement by van der Pauw method (right, c).

2.6. Structural characterization, Raman and elemental analyses of p-, B- and n-CNT-WF$_{(t)}$

CNT papers are inspected by scan electron microscope (SEM, Hitachi-SU8010) which gives information regarding to surface texture and CNT distribution. Raman is a powerful tool widely used to characterize carbon structures based on D and G-bands; the former appears as a result of phonon scattering at zone boundaries (A_{1g} mode = 1375 cm^{-1}) and becomes strong as defect density increases. The latter comes from C–C bond stretching (E_{2g} mode = 1583 cm^{-1}) and is present in all sp^2 bonded structures. Accordingly, the degree of graphitization can be characterized by I_D/I_G where I_D and I_G represent intensity of D and G-bands.[19] In this work, Raman spectra of CNTs papers are recorded by Horiba-HR800 at room temperature and bonding characters are analysed using X-ray photoelectron emission spectroscopy (XPS, ULVAC-PHI PHI 5000 Versaprobe II); the XPS peak intensity is calculated according to the full width at half maximum and elemental ratio (Q_x) of C 1s, O 1s, N 1s and B 1s spectra expressed as $Q_x = n_x/\Sigma n_i = (S_x/X_x)/\Sigma(S_i/X_i)$ where X_x is corrected relative sensitivity factor and S_x is signal intensity.[20]

2.7. Work function and Hall effect measurements of p-, B- and n-CNT-WF$_{(t)}$

The work function (Φ) of CNT papers is calculated according to equation $\Phi = h\nu - E_o - E_F$ where excitation energy ($h\nu$), secondary electron cut-off energy (E_o) and the Fermi energy (E_F) are determined by tangential equation and ultraviolet photoelectron spectroscopy (UPS) at $h\nu = 21.22$ eV. The Φ and UPS are only calculated and recorded for samples made with p-CNT-WF, n-CNT-WF and B-CNT-WF (ESI 1†). Carrier concentration of CNT papers is probed by Hall-effect measurement system using 80–350 K and 15 × 15 mm sample kit (Ecopia, HMS 5000). Fig. 2c shows working principe (left) and setup of Hall effect measurement (right) based on the van der Pauw method where Hall voltage (V_H) and Hall coefficient (R_H) are expressed as $V_H = V_A + V_B + V_C + V_D$ (Fig. 2a) and $R_H = V_H a/I_x B$ (a, B and I_x denote sample thickness, magnetic field and current in x direction).

3 Results and discussion

Fig. 3a shows a SEM image of p-CNT-WF, along with the ρ–f_{CNT} plot (insert). Clearly, the WF structure is of band-like and ranges at 5–30 μm in width and 0.7–1.2 mm in length (ESI 2†). It is worth mentioning that papers made of pure CNTs lack sustainable strength and dissociate rapidly with stressing (*e.g.* handling and sampling). Addition of WFs into CNTs truly improves paper strength, as evident by stress–strain curve

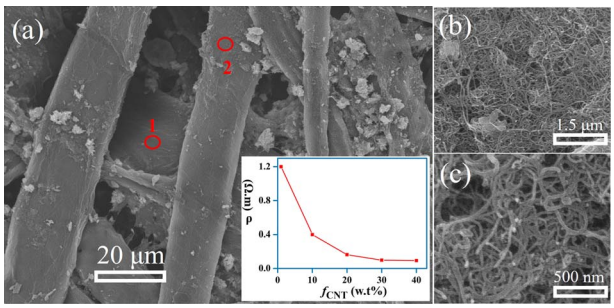

Fig. 3 SEM image of p-CNT-WF. Insert: the ρ–f_{CNT} plot of p-CNT-WF (a). Enhanced SEM images of circles 1 and 2 (b and c).

Table 1 Elemental content of all samples studied

	Elements (at%)			
Samples	O	C	N	B
p-CNT-WF	32.94	66.61	0.41	0.05
n-CNT-WF$_{(10min)}$	34.36	63.14	2.43	0.07
n-CNT-WF$_{(20min)}$	34.98	61.97	2.98	0.06
B-CNT-WF	40.51	56.97	0.72	1.8
B-CNT-WF$_{(10min)}$	35.19	61.63	1.82	1.36
B-CNT-WF$_{(20min)}$	39.95	55.35	2.77	1.92

where tensile strength reaches 15.8 MPa; a value which is comparable with oxides based flexible devices (ESI 3†).[10] Four-terminal measurements and SEM images verify the p-CNT-WF to be electrically conductive with η-f_{CNT} = 20 wt%; (i) ρ decreases rapidly at f_{CNT} = 10–20 wt% (insert, Fig. 3a); (ii) CNTs network on WFs (circles 1 and 2, Fig. 3b and c). Accordingly, all characterizations are carried out on conductive papers made of f_{CNT} = 20 wt%. Electrical measurements carried out along in-plane and out-of-plane directions of p-CNT-WF confirm the ρ difference to be as low as 0.05 Ω m (ESI 4†). SEM images however fail to identify structural alternation of CNTs before and after plasma treatments (ESI 5†).

Fig. 4a shows Raman spectra and calculated I_D/I_G where hydrogenated amorphous carbon often seen in pyrolysis made CNTs is also present (*a*: C–H = 1587 cm^{-1}).[19] Clearly, the I_D/I_G increases with plasma treatments, indicative of surface modification enhanced A_{1g} mode.[19] Table 1 lists content of O 1s, C 1s, N 1s and B 1s according to deconvoluted XPS spectra where bonding characters are identified to be C=C (284.7 eV), C=O (531.2 eV), C–O (532.4 eV), O–C=O (533.4 eV), graphitic-N (NQ, 401 eV), pyridinic-N (N6, 398.3 eV), B–N (190.6 eV), C–B (191.2 eV) and B–O (192.2 eV) (ESI 6–8†).

First, the O 1s content increases while C 1s decreasing, indicative of oxygenation through reactions of absorbed O_2 with carbon lattices (*i.e.* conversion of C=C into C–O, C=O and O–C=O).[20] Second, N_2 plasma induced nitridation is evident by increased N 1s content in n-CNT-WF$_{(10min)}$ and n-CNT-WF$_{(20min)}$. Third, conversion of p-CNT-WF into B-CNT-WF is supported by (i) B–C bond formation (191.2 eV) and increased B 1s content (ESI 8†); (ii) C 1s and B 1s mapping analyses (Fig. 4b–d); (iii) B–N bond formations (190.6 eV, ESI 8†). Additional evidence in support of p → n conversion comes from Φ and Hall-effect measurements; the former shows a decrease by 15–16% and is attributed to electronegativity from lone pairs of O and N (Table 2).

The latter displays a transition from hole- to electron-governed carriers, indicative of both O and N acting as n-dopants. It is worth mentioning for an electron–hole

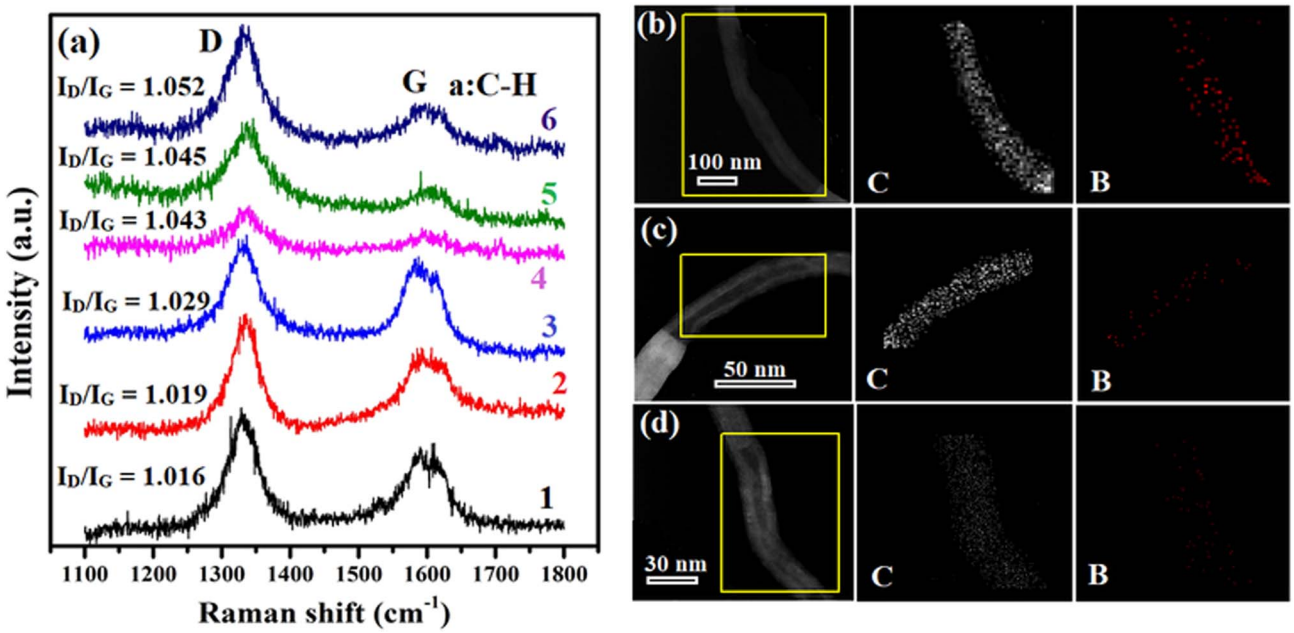

Fig. 4 Raman spectra and I_D/I_G of all samples where curve 1–6 stands for p-CNT-WF, n-CNT-WF$_{(10min)}$, n-CNT-WF$_{(20min)}$, B-CNT-WF, B-CNT-WF$_{(10min)}$ and B-CNT-WF$_{(20min)}$ (a). The C and B mapping on individual B-CNTs (b–d).

Table 2 Φ and carrier concentration/mobility of samples studied

Samples	Φ (eV)	Carrier con. (cm^{-2})	Mobility ($cm^2\ V^{-1}\ s^{-1}$)
p-CNT-WF	4.62	5.642×10^{13}	1303.3
n-CNT-WF$_{(10min)}$	3.86	-2.47×10^{13}	2691.9
n-CNT-WF$_{(20min)}$	3.92	-5.92×10^{13}	1099.7
B-CNT-WF	5.22	9.8×10^{13}	797.2

symmetric semiconductor that E_F lies at the middle of E_g between valence (VB) and conduction band edge (CB). Doping, however, creates localized states near to band edge, for example, n-/p-doped states appear in the vicinity of CB/VB edge. In this case, the localized states become the new edge and E_F needs to be redefined.[8]

Fig. 5a shows band diagram of p-CNT-WF where E_F lies at the middle of E_g between VB and p-doped state arising from electron-deficient defects.[8] N_2 plasma creates n-doped state near to the CB so E_F is lifted and a ΔE forms between p- and n-CNT-WF$_{(t)}$ (Fig. 5a and b). B-Doping enhances p-type character and moves p-doped state much closer to VB so Φ increases and ΔE becomes greater (Fig. 5b and c & Table 2). It is worth mentioning that carrier concentration and mobility uncovered here are consistent with reported data on CNTs (Table 2).[8]

Since diodes are unidirectional conductors, the p- and n-sides of p-CNT-WF/p-CNT-WF, p-CNT-WF/n-CNT-WF$_{(t)}$ and B-CNT-WF/n-CNT-WF$_{(t)}$, made of $f_{CNT} = 20$ wt% (insert, Fig. 3a), are connected to positive and negative electrodes of a power supply (*i.e.* the forward bias direction, yellow arrows, Fig. 5). Fig. 6 displays *I–V* curves of p-CNT-WF/p-CNT-WF (a), p-CNT-WF/n-CNT-WF$_{(10min)}$ (b) and p-CNT-WF/n-CNT-WF$_{(20min)}$ (c) where profiles recorded at the 3rd (*i.e.* negative region) are also superimposed on the 1st quadrant to highlight diode character (*i.e.* positive region and orange). Clearly, a symmetric *I–V* curve is present in p-CNT-WF/p-CNT-WF with $R_R/R_F = 1.05$, indicative of an ohmic conductor (Fig. 6a). Asymmetric profiles however are present in p-CNT-WF/n-CNT-WF$_{(10min)}$ and p-CNT-WF/n-CNT-WF$_{(20min)}$; the latter resembles a diode and the R_R/R_F, I_F and V_{th} are measured to be 2.01, 165 nA and 1.9 V. This value is lower than that of Si based ($I_F = 10^{-3}$–10^{-5} A and $V_{th} = 0.5$–0.7) and is due to fact that conductive papers are made from a large number of CNTs connected in parallel, *i.e.* $V_{th} = V_1 = V_2 = V_3$ & $I_F = I_1 + I_2 + I_3 \ldots$ where V_n and I_n denote V and I contribution by

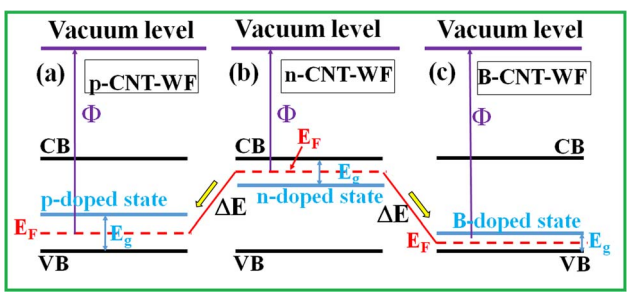

Fig. 5 Band diagrams of p-CNT-WF (a), n-CNT-WF (b) and B-CNT-WF (c); yellow arrows indicate forward bias direction.

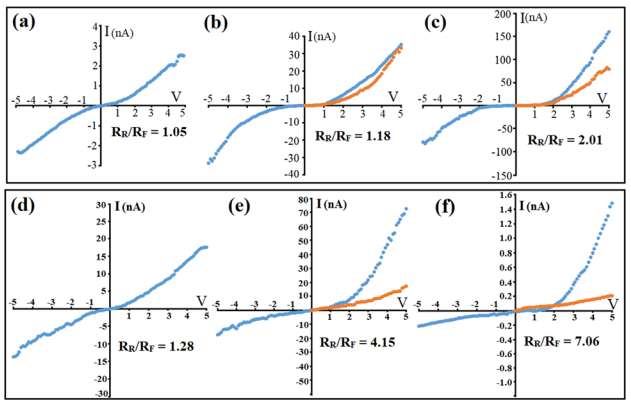

Fig. 6 *I–V* profiles of p-CNT-WF/p-CNT-WF (a), p-CNT-WF/n-CNT-WF$_{(10min)}$ (b), p-CNT-WF/n-CNT-WF$_{(20min)}$ (c), B-CNT-WF/B-CNT-WF (d), B-CNT-WF/n-CNT-WF$_{(10min)}$ (e) and B-CNT-WF/n-CNT-WF$_{(20min)}$ (f); all samples are made of $f_{CNT} = 20$ wt%.

individual tubes.[21,22] A similar trend is also observed in B-CNT-WF/B-CNT-WF and B-CNT-WF/n-CNT-WF$_{(10min)}$ with $R_R/R_F = 1.28$ and 4.15; the latter again verifies B-doping enhanced p-character (Fig. 6d and e). Surprisingly, the R_R/R_F reaches 7.06 for B-CNT-WF/n-CNT-WF$_{(20min)}$ (Fig. 6f); a value which is comparable with conventional Si-based devices and is consistent with Fig. 5 & Table 2. Abbreviation in manuscript are list in Table 3.

Table 3 Abbreviation list

Abbreviation	Full name
ΔE	Built-in-potential
E_F	Fermi levels
DL	Depletion layer
d	Tube diameter
θ	Tube chirality
a_{c-c}	C–C bond length
E_g	Band gap
f_{CNT}	Filling fraction
WFs	Wood fibres
ρ	Electrical resistivity
a	Paper thickness
η	Electrical percolation threshold
V_{th}	Threshold voltage
I_F	Maximum forward current
R_R	Reverse resistance
R_F	Forward resistance
I_D	Intensity of D band
I_G	Intensity of G band
Q_x	Elemental ratio
X_x	Corrected relative sensitivity factor
S_x	Signal intensity
Φ	Work function
hv	Excitation energy
V_H	Hall voltage
R_H	Hall coefficient
I_x	Current in x direction
B	Magnetic field
VB	Valence band
CB	Conduction band

4 Conclusions

Flexible conductive papers are made from CNTs and WFs. As-made papers behave as p-type and can be changed into n-type through N_2 plasma treatments. Elemental analyses confirm formation of graphitic N structure after N_2 plasma treatments thus reducing ϕ from 4.62 to 3.86 eV. The B-doping enhances p-type character so ϕ increases to 5.22 eV. By screening one face of p-CNT-WF in plasma, p–n junctions are successfully created along paper thickness direction and are verified by electrical rectification and $R_R/R_F \gg 1$. The R_R/R_F of B-CNT-WF/n-CNT-$WF_{(20min)}$ reaches a value as high as 7.06.

Conflicts of interest

The authors declare no conflict of interest.

Acknowledgements

Authors thank the National Science and Technology Council (NSTC) of Taiwan for the financial support (MOST-110-2112-M-007-014). Authors also acknowledge the use of F200 HRTEM and ARM200 Cs TEM which belong to Instrumentation Centre at National Tsing-Hua University (NTHU) under funding by the National Science and Technology Council (NSTC) of Taiwan.

References

1 B. D. Gates, Flexible Electronics, *Science*, 2009, **323**, 1566–1567.
2 Y. G. Gurevich and G. N. Logvinov, Physics of thermoelectric cooling, *Semicond. Sci. Technol.*, 2005, **20**, R57.
3 P. R. Wilson, Measurements on the depletion layer properties of planar diodes, *Solid-State Electron.*, 1969, **12**, 539–547.
4 J. Hu, M. Ouyang, P. Yang and C. M. Lieber, Controlled growth and electrical properties of heterojunctions of carbon nanotubes and silicon nanowires, *Natur*, 1999, **399**, 48–51.
5 C. Zhou, J. Kong, E. Yenilmez and H. Dai, Modulated Chemical Doping of Individual Carbon Nanotubes, *Science*, 2000, **290**, 1552–1555.
6 M. S. Dresselhaus, G. Dresselhaus and A. Jorio, UNUSUAL PROPERTIES AND STRUCTURE OF CARBON NANOTUBES, *Annu. Rev. Mater. Res.*, 2004, **34**, 247–278.
7 T. W. Ebbesen, H. J. Lezec, H. Hiura, J. W. Bennett, H. F. Ghaemi and T. Thio, Electrical conductivity of individual carbon nanotubes, *Natur*, 1996, **382**, 54–56.
8 K. Liu, P. Avouris, R. Martel and W. K. Hsu, Electrical transport in doped multiwalled carbon nanotubes, *Phys. Rev. B: Condens. Matter Mater. Phys.*, 2001, **63**, 161404.
9 J. B. Bult, R. Crisp, C. L. Perkins and J. L. Blackburn, Role of Dopants in Long-Range Charge Carrier Transport for p-Type and n-Type Graphene Transparent Conducting Thin Films, *ACS Nano*, 2013, **7**, 7251–7261.
10 J. E. Cha, S. Y. Kim and S. H. Lee, Effect of Continuous Multi-Walled Carbon Nanotubes on Thermal and Mechanical Properties of Flexible Composite Film, *Nanomaterials*, 2016, **6**, 182.
11 P. G. Collins, K. Bradley, M. Ishigami and A. Zettl, Extreme Oxygen Sensitivity of Electronic Properties of Carbon Nanotubes, *Science*, 2000, **287**, 1801–1804.
12 S. Durukan and F. Karadagli, Physical characteristics, fiber compositions, and tensile properties of nonwoven wipes and toilet papers in relevance to what is flushable, *Sci. Total Environ.*, 2019, **697**, 134135.
13 W. K. Hsu, S. Y. Chu, E. Muñoz-Picone, J. L. Boldú, S. Firth, P. Franchi, B. P. Roberts, A. Schilder, H. Terrones, N. Grobert, Y. Q. Zhu, M. Terrones, M. E. McHenry, H. W. Kroto and D. R. M. Walton, Metallic behaviour of boron-containing carbon nanotubes, *Chem. Phys. Lett.*, 2000, **323**, 572–579.
14 W. Han, Y. Bando, K. Kurashima and T. Sato, Boron-doped carbon nanotubes prepared through a substitution reaction, *Chem. Phys. Lett.*, 1999, **299**, 368–373.
15 J.-J. Zeng and Y.-J. Lin, Tuning the work function of graphene by nitrogen plasma treatment with different radio-frequency powers, *Appl. Phys. Lett.*, 2014, **104**, 233103.
16 J. Duch, P. Kubisiak, K. H. Adolfsson, M. Hakkarainen, M. Golda-Cepa and A. Kotarba, Work function modifications of graphite surface via oxygen plasma treatment, *Appl. Surf. Sci.*, 2017, **419**, 439–446.
17 D. W. Koon and C. J. Knickerbocker, What do you measure when you measure resistivity?, *Rev. Sci. Instrum.*, 1992, **63**, 207–210.
18 P. S. Na, H. Kim, H.-M. So, K.-J. Kong, H. Chang, B. H. Ryu, Y. Choi, J.-O. Lee, B.-K. Kim, J.-J. Kim and J. Kim, Investigation of the humidity effect on the electrical properties of single-walled carbon nanotube transistors, *Appl. Phys. Lett.*, 2005, **87**, 093101.
19 M. S. Dresselhaus, G. Dresselhaus, R. Saito and A. Jorio, Raman spectroscopy of carbon nanotubes, *Phys. Rep.*, 2005, **409**, 47–99.
20 J.-L. Li, K. N. Kudin, M. J. McAllister, R. K. Prud'homme, I. A. Aksay and R. Car, Oxygen-Driven Unzipping of Graphitic Materials, *Phys. Rev. Lett.*, 2006, **96**, 176101.
21 J. P. McKelvey, *Solid state and semiconductor physics*, Harper & Row, 2018.
22 P. C. P. Watts, W.-K. Hsu, H. W. Kroto and D. R. M. Walton, Are Bulk Defective Carbon Nanotubes Less Electrically Conducting?, *Nano Lett.*, 2003, **3**, 549–553.